International Journal of Biological Macromolecules 282 (2024) 136557

Contents lists available at ScienceDirect

International Journal of Biological Macromolecules

journal homepage: www.elsevier.com/locate/ijbiomac

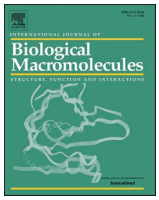

Polyurethane infused with heparin capped silver nanoparticles dressing for wound healing application: Synthesis, characterization and antimicrobial studies

Jayshree H. Ahire [a,*], Qi Wang [b], Gary Rowley [c], Isabelle Chambrier [a], Jason C. Crack [a], Yongping Bao [b], Yimin Chao [a]

[a] School of Chemistry, University of East Anglia, United Kingdom
[b] Norwich Medical School, University of East Anglia, United Kingdom
[c] School of Biological Sciences, University of East Anglia, United Kingdom

ARTICLE INFO

Keywords:
Infections
Wound healing
Silver nanoparticles
Heparin
Polyurethane
Electrospinning
Antibacterial

ABSTRACT

Burn and diabetic wounds present significant challenges due to their complex nature, delayed healing, pain, and high susceptibility to bacterial infections. In this study, we developed and evaluated polyurethane (PU) nanofibers embedded with heparin-functionalized silver nanoparticles (hep-AgNPs) using an electrospinning technique. The choice to functionalize silver nanoparticles with heparin was based on heparin's established role in modulating inflammation and promoting angiogenesis. The electrospun nanofibers exhibited smooth, bead-free morphology with diameters ranging from 300 to 500 nm and demonstrated a sustained release of silver over seven days, offering continuous antimicrobial protection.

Mechanical testing of the nanofibers revealed excellent strength and elasticity, making them well-suited for flexible wound dressings. The nanofibers also showed superior water absorption, fluid retention, and controlled water vapor transmission, essential for maintaining a moist wound environment conducive to healing. In vitro biocompatibility assays confirmed that the PU/hep-AgNPs bandages were non-toxic to keratinocytes and fibroblasts and significantly accelerated wound closure, as evidenced by scratch assays. The nanofibrous bandages also exhibited potent antibacterial activity against *Staphylococcus aureus* and *Salmonella Typhimurium*, two common wound pathogens.

Overall, our findings demonstrate that PU/hep-AgNPs nanofibrous bandages are a promising candidate for chronic wound healing. They combine excellent biocompatibility, anti-inflammatory properties, and strong antimicrobial activity, which collectively contribute to faster wound healing and reduced risk of infection.

1. Introduction

Infections are considered a global public health issue and are the main reason why most people die from burns and diabetic wounds. Nowadays treating wound infections through traditional antibiotics is a major clinical challenge, requiring a novel shift to improve chronic wound care. The United States government estimates that about 23,000 people die per year as a result of infection from drug-resistant bacteria [1]. The US Center for Disease Control has predicted more deaths from antimicrobial-resistant bacteria than from all types of cancers combined by 2050 [2]. Thus, there is an urgent need to develop new wound dressing materials that do not rely on antibiotics. Wound healing is a complex regenerative process and to ensure their effectiveness wound dressings need to address several criteria: 1) maintain a moist wound environment, 2) promote gas exchange, 3) be easy to remove without pain or trauma, 4) provide mechanical protection and 5) accelerate wound healing with or without the presence of non-toxic antibacterial agents [3]. However, for long healing processes the antimicrobial property is the most important factor that protects wounds from microorganisms. Even when the dressing encloses the wound, bacterial infection can still occur due to the moist environment trapped inside which provides space and nutrients for microorganisms to grow [4]. To avoid this situation, disinfectant agents have been introduced such as curcumin, chitosan and silver nanoparticles (AgNPs) [5].

* Corresponding author.
E-mail address: j.ahire@uea.ac.uk (J.H. Ahire).

https://doi.org/10.1016/j.ijbiomac.2024.136557
Received 31 May 2024; Received in revised form 7 October 2024; Accepted 11 October 2024
Available online 18 October 2024

Among these, AgNPs are most recognized for their excellent antimicrobial properties and have been most explored in the last two decades leading to their use in food packaging [6], as scaffolds for tissue engineering [7,8], filters [9], coatings [10], in wound dressings etc. [11–13] Due to the small size of AgNPs, they readily penetrate microbial cells. Once internalized into the microbial cell, AgNPs result in the upregulation of heat shock proteins, inductive of protein denaturation. The thiophilic nature of Ag(I) ions also leads to the disruption of iron-sulfur assembly as well as perturbations in iron, copper and sulfur homeostasis. Ag(I) ions are also redox active and capable of inducing redox stress [10,14]. In turn these processes damage the DNA and the cell membrane, ultimately resulting in bacterial cell death [14,15]. Some AgNPs also possess antifungal or antineoplastic properties, and in some cases are also phytotoxic [16,17]. Moreover, AgNPs have been shown to effectively penetrate and disrupt bacterial biofilms which are communities of bacteria encased in a self-produced extracellular matrix [18]. By inhibiting biofilm formation and destabilizing existing biofilms, silver nanoparticles prevent the colonization and persistence of bacterial infections. While AgNPs offer significant potential for various applications, including wound dressings, medical implants, and antimicrobial coatings, their potential toxicity necessitates careful consideration. Although debates exist regarding Ag use in wound healing, recent studies indicate that AgNPs can be effective when dosage and release are carefully controlled, minimizing toxicity while harnessing antimicrobial properties. Wound-dressing products that include AgNPs are commercially available for use in wound-healing therapy [19,20]. These silver based dressings have not shown adverse effects during extended therapy, and several products, like Aquacel Ag®, DynaGinateTM (Ag calcium alginate dressing), CuraFoamTM, DynaGinateTM (Ag foam dressing), and SilverIon®, are commercially available [21]. Moreover, silver nanoparticles combined with biopolymers are widely recognized as safe bionanomaterials [22]. Despite challenges, other nanoparticles, such as gold, iron oxide, titanium oxide, zinc oxide, and copper, are also recommended for wound healing applications [23–27]. Further research is needed to better understand the mechanisms underlying the toxicity of silver nanoparticles, establish safe exposure limits, and develop effective risk management strategies to ensure their safe use in consumer products and medical applications.

The incorporation of AgNPs into polymeric membranes is considered as one of the natural solutions for the development of bandages for wound dressings [28]. The polymeric membrane or material helps to safely remove the bandage or frequent dressing from the newly regenerated tissue without causing damage to the wound. In recent years, biomaterial-based wound dressings have attracted a lot of attention due to their excellent biocompatibility, easy availability, non-toxic nature, biodegradability and moisture absorptive property. There are a variety of polymers used in biomedical applications, with polyurethane (PU) commonly used for the preparation of wound dressings. PU copolymers have been successfully employed as a biomaterial ranging from heart catheters to orthodontic applications, due to their excellent physicomechanical properties, good biocompatibility and high flexibility [29,30].

PU is ideal for wound dressing due to its good barrier properties and oxygen permeability, which are important for membrane applications. PU copolymer is synthesized from hard and soft segments which can impart a wide range of physical and chemical properties to the final material, therefore careful selection of the constituent chemistry and types of components used in the syntheses of the PU polymers can lead to the generation of biocompatible PUs [31]. Moreover, suitable mechanical property to maintain flexibility and integrity, besides good hydrophilicity and water uptake in order to have wound healing ability, is an essential requirement for developing the wound healing dressing [32]. PU combined with an electrospinning method is expected to have synergistic advantage in wound care applications. Electrospun nanofibers have been reported to possess potential for wound dressings such as high porosity effectively contributing to gas exchange, providing the required oxygen for cell respiration and fluid absorption [33]. Their excellent mechanical and physical properties as well as elasticity, make them flexible enough to accommodate body movement while serving as a protective barrier against the environment. Additionally, drugs and active agents can be easily incorporated into these fibers [34]. Compared to other wound dressings like hydrogels and sponges [35,36], electrospun PU fibers provide superior mechanical support, conformability, and controlled drug release, closely mimicking the extracellular matrix to enhance healing outcomes. In contrast, hydrogels excel in moisture retention but lack mechanical strength, while sponges are effective at absorbing exudates but don't offer the same level of controlled drug release or flexibility as electrospun fibers.

Heparin has been extensively studied and commercialised mainly due to its anticoagulant and antithrombotic properties in medicine. It is also well studied and still used in other therapeutic applications such as wound healing, burn injury treatment, inhibition of inflammation and metastatic spread of tumour [37–40]. Heparin is polydisperse sulphated glycosaminoglycan that can be obtained from porcine or bovine intestinal mucosa, and is widely used in the treatment and prevention of thrombotic events. The structural properties of heparin allow it, and its derivatives, to selectively interact with multiple cellular targets, leading to a wide array of biological effects, e.g. anticoagulant, anti-inflammatory, anti-tumour and angiogenesis [41–43]. Consequently, it is also well studied and used in other therapeutic applications such as wound healing, burn injury treatment, inhibition of inflammation and metastatic spread of tumour [37,40]. The exact mechanism underlying the antibacterial activity of heparin is not fully understood, but several hypotheses have been proposed. Heparin may interact with bacterial membranes, leading to destabilization and permeabilization, resulting in leakage of cellular contents and ultimately bacterial cell death [44]. Heparin has been shown to interfere with the adhesion of bacteria to host cells by blocking bacterial attachment consequently preventing the establishment of infection and aiding in bacterial clearance by the immune system [45]. Heparin has also been shown to boost the immune response against bacterial infections by enhancing the activity of immune cells like macrophages and neutrophils, aiding in the clearance of bacterial pathogens. Heparin has been reported to disrupt bacterial biofilms, making bacteria more vulnerable to antibiotics and immune attack [46,47]. Overall, while the antibacterial activity of heparin is not as well-characterized as its anticoagulant effects, the emerging evidence suggests that it possesses significant potential as an antimicrobial agent. Further research is needed to elucidate the underlying mechanisms of heparin's antibacterial activity and explore its potential therapeutic applications in the prevention and treatment of bacterial infections.

In this study, we developed a novel wound dressing material by embedding heparin-functionalized silver nanoparticles (hep-AgNPs) into polyurethane using electrospinning. This innovative approach combines the antibacterial properties of AgNPs with heparin's anti-inflammatory and pro-angiogenic effects, offering a more comprehensive treatment for wound healing. Unlike traditional AgNP-based materials, hep-AgNPs address both infection and inflammation, enhancing overall efficacy. Heparin's stabilization of AgNPs ensures prolonged silver ion release, and its negative charge facilitates bacterial cell entry, intensifying the antibacterial impact. Additionally, heparin inhibits bacterial biofilm formation, further preventing chronic infections. Our study thoroughly assessed the physical properties, biocompatibility, and antimicrobial effects of hep-AgNPs, demonstrating their superior potential in treating infected wounds, chronic wounds, and other biomedical applications.

2. Materials and method

2.1. Materials

Silver nitrate ($AgNO_3$) and dimethylaminopyridine (DMAP) were purchased from Fisher Scientific, UK. Sodium borohydride ($NaBH_4$), 2-

mercaptoethylamine hydrochloride (cysteamine), *N*-(3-dimethylaminopropyl)-*N*′-ethylcarbodiimide hydrochloride (EDC), *N*-hydroxysuccinimide (NHS), tetrahydrofuran (THF), *N*,*N*-dimethylformamide (DMF), Heparin Sodium salt from porcine mucosa, dimethyl sulfoxide (DMSO) and 3-(4,5-dimethyl-2-thiazolyl)-2,5-diphenyl tetrazolium bromide (MTT) were purchased from Sigma-Aldrich. PU (Z3A1) was purchased from Biomer technologies, Cheshire, UK. Water was purified using a milli-Q (18.2 MΩ) reagent-grade water system from Purelab Flex. L929 cells were generously supplied by Dr. Linda Troeberg from UEA, while HaCat cells were provided by Dr. Chris Morris from UCL.

2.2. Cysteamine capped silver nanoparticles (cyst-AgNPs)

Cysteamine-capped silver nanoparticles (cyst-AgNPs) were synthesized using a method published by Oliva et al. [48] In a typical reaction preparation, DMF (20 ml) was added into an erlenmeyer flask along with a magnetic stirrer bar. The flask was kept in an ice-bath and an aqueous solution of cysteamine (0.7 mmol, 0.5 ml) and $AgNO_3$ (0.234 mmol, 0.5 ml) were sequentially added. The reaction mixture was stirred for 10 min, then an aqueous solution of $NaBH_4$ (3 ml, 210 mM) was added dropwise. An immediate color change was observed from milky white to yellowish brown. The reaction mixture was stirred for 30 min. The cyst-AgNPs were collected and purified by washing 3 times with DMF by centrifugation (8000 rpm, 10 min) and re-suspended into water.

2.3. Synthesis of heparin capped silver nanoparticles (hep-AgNPs)

Heparin capped AgNPs were synthesized using an amide-coupling reaction. A mixture of heparin sodium salt (2 eq, 48 mg), EDC (8 eq), NHS (8 eq) and a catalytic amount of DMAP were added into a 25 ml round bottom flask and stirred at RT in the presence of water (5 ml). After 2-h cyst-AgNPs (1 eq, 24 mg) were added into the reaction mixture and stirred overnight. The resulting reaction mixture was precipitated using ethanol and ice-cold diethyl ether to remove the excess of coupling reagents and by-products. The reaction mixture was centrifuged (10,000 rpm) for 10 min and washed 3 times with ethanol and diethyl ether. The obtained hep-AgNPs were re-dispersed into water before characterization.

2.4. Nanofiber formulation using electrospinning

Commercially bought PU (10 % *w/v*) was dissolved in a DMF-THF (7:3 ratio respectively) solvent mixture, total volume of 10 ml [49,50]. Different concentrations of hep-AgNPs (1 %, 3 %, 6 % and 10 % (*w/v*)) were added to the PU (10 % w/v) polymer solution and left on a shaker overnight to obtain a homogeneous solution. Prior to electrospinning, the mixture of PU and hep-AgNPs (10 ml) was loaded into a hamilton syringe with blunt tipped stainless steel 21G needle. The nanofibers were created at constant feed rate of 40 μl/min using a programmable syringe pump (Cole-Parmer) with an accelerating voltage of 15 kV supplied by a high voltage power supply (Gamma High Voltage Research Ormond Beach, FL). Different concentrations of nanofibers samples were formulated similarly.

2.5. Characterization of silver nanoparticles

Heparin capped AgNPs and cysteamine terminated silver nanoparticles were characterized by UV–vis absorption spectroscopy, Fourier transform infrared (FTIR) spectroscopy, scanning electron microscopy (SEM), Energy-dispersive X-ray spectroscopy (EDX) and dynamic light scattering (DLS) measurement.

The UV–vis absorption spectra of hep-AgNPs and cyst-AgNPs were recorded on a PerkinElmer 35 UV–vis double-beam spectrometer in a quartz cuvette (10 × 10 mm). FTIR measurements were carried out using a PerkinElmer ATR-FTIR spectrometer from the solid samples of hep-AgNPs and cyst-AgNPs. The hydrodynamic diameter and polydispersity index of hep-AgNPs and cyst-AgNPs were determined by DLS measurement with a Zetasizer Nano ZS (Malvern Instruments Ltd., UK). The SEM and EDX measurements were carried out using Zeiss Gemini 300 SEM (with a Quorum technologies cryo system; an Oxford instruments EDS and STEM and Inlens detectors). The nanoparticles samples were prepared by drop-casting a dilute suspension of the AgNPs in ethanol onto a 200-mesh carbon-coated copper grid. The grids were dried before the measurement and the micrographs were taken at different spots on the grids. The nanofibers bandage samples were imaged after gold coating. The fiber diameters and pore sizes were quantified from SEM images of three different bandage samples.

2.6. Evaluation of mechanical properties

The mechanical properties of the nanofibers bandages (1.5 × 0.5 cm) were assessed using a tensiometer (Instron 34TM-30). A 500 N load cell was used to perform a ramp test for each sample at a rate of 0.125 mm/s. The size and thickness of each sample were used to report the ultimate tensile strength (UTS) and the Young's modulus (YM) in N/mm.

2.7. Assessment of swelling ratio (SR)

The swelling ratio or absorbency test of the nanofibers bandages was determined by the method established for ideal wound dressing material (BS EN 13726-1: 2002). Briefly, the nanofibers bandage samples were cut into a circle with a diameter of 16 mm and weighed (W_1), then submerged into 10 ml of PBS solution at 37 °C for 24 h to reach maximum swelling equilibrium. The samples were then removed, gently shaken and wiped to remove freely draining liquid, and the samples reweighed (W_2). The absorbency of the sample was calculated using the following equation:

$$\mathrm{SR} = \frac{W_2 - W_1}{\text{area } (\mathrm{cm}^2)}$$

2.8. Water contact angle

The wettability test of the electrospun nanofibers bandages with and without hep-AgNPs was assessed using a TBU with OCA 50 from Data Physics instrument, employing a sessile drop test technique. The analysis of the data was performed using SCA20 software.

2.9. Fluid retention (FR)

To calculate the fluid retention capacity/high compression capacity of the nanofibers bandages, the hydrated sample was placed onto a perforated metal sheet and 40 mmHg pressure was applied to the sample. Any remaining liquid was allowed to drain and wiped out; the sample was then reweighed (W_3). The fluid retention was calculated using the following equation:

$$\mathrm{FR} = \frac{W_3 - W_1}{\text{area } (\mathrm{cm}^2)}$$

2.10. The water vapor transmission rate (WVTR) assay

The water vapor transmission rate (WVTR) of the nanofibers bandages was determined according to ASTM E96-00 protocol. Nanofibers bandage samples were used to seal over the circular opening of glass tubes containing 4 ml of PBS. The diameter of the tube was 15 mm, the tube was kept in an incubator with a constant temperature of 37 °C and 85 % chamber humidity which contains a saturated solution of ammonium sulfate. The WVTR ($g/m^2 \cdot day$) was calculated as:

$$\mathrm{WVTR} = \frac{W_i - W_t}{A \times t}$$

where A represents the area of the tube's mouth (m^2), t is the trial time and Wi and Wt are the weights of trial before and after, respectively.

2.11. Silver release study from nanofibers

The silver release study of the nanofibers bandages was performed according to the method reported by Maneerung and Rigo et al. [51] The Ag content was determined using an inductively coupled plasma mass spectrometer (A Thermo iCAP™ TQ-ICP-MS technique). A sample of nanofibers bandage sheet weighing 0.1 g was dispersed into a corning tube containing 10 ml of PBS solution. The tube was then placed into a water bath at 37 °C with a shaking speed of 120 rpm/min. All the samples were prepared following a similar method and at predetermined time intervals (0, 0.5, 1.0, 3.0, 6.0, 12, 24, 56, 72, 96, 120 h, 6 and 7 days) the medium was removed and refreshed with an equivalent amount of PBS. The solutions were then acidified with 2 % nitric acid to ensure that all the silver released remained in solution. The suspending fluids from the predetermined time interval were then analyzed for silver ions by ICP-MS. The amount of silver content was calculated and presented as a function of time. Each experiment was carried out in triplicate.

2.12. Cell culture

The potential cytotoxicity of the nanofibers wound healing bandages were assessed using the keratinocyte HaCat cell lines and mice fibroblast L-929 cell line. The cells were cultured in DMEM supplemented with 1 % penicillin–streptomycin (Gibco, UK), 1 % L-Glutamine (200 mM, Gibco, UK) and 10 % fetal bovine serum (FBS; Gibco, US) for 5–7 days in 75 cm^2 cell culture flasks (Thermos Fisher, UK) at 37 °C in a 5 % CO_2 humidified environment. Following culture, the cells were detached using trypsin-EDTA treatment and seeded at a density of 5×10^3 cells per well in 96-well cell culture plates (Thermos Fisher, UK). After 24 h, the culture medium was replaced with either fresh DMEM media or nanofiber sample solutions and subsequently, the cells were further incubated for 24 h to assess any cytotoxic effects.

2.13. Evaluation of cytotoxicity

The in vitro cytotoxicity of nanofibers bandages was assessed using a MTT assay. This method determines the mitochondrial dehydrogenase activity to evaluate cell viability. Briefly, a sterile filtered MTT stock solution in phosphate-buffered saline (PBS) at pH 7.4 (5 mg/ml) was added into 96 well plate, achieving a final concentration of 0.5 mg/ml^{-1}. After 2 h of incubation, the unreacted dye was removed, and the insoluble formazan crystals were dissolved in 100 μl of DMSO. The absorbance was then quantified at a wavelength of 540 nm using a reference wavelength of 630 nm by microplate reader (BMG Labtech Ltd., UK). Relative cell viability (%) was determined using the following formula:

$$\text{Cell viability } (\%) = OD_{test}/OD_{control} \times 100\%$$

2.14. Wound healing assay

HaCat Cells were seeded in 12-well plates at 2×10^5 cells/well. After the cells reached 90 % confluence, scratches were made with a 200 μl pipette tip across the center of the wells without changing the medium. Detached cells were removed by gently washing twice with the medium. The wells were then filled with fresh medium containing different treatments. The cells were grown for a further 24 h, while images of the wound area were taken on a BioTek Cytation 7 (Agilent, US) at 4× magnification. The wound area was analyzed using ImageJ software.

2.15. Antimicrobial activity

The in vitro antibacterial activity of the nanofibers hep-AgNPs/PU bandages samples with various amounts of Ag content was evaluated against the Gram-positive bacteria *Staphylococcus aureus* (NCTC 12973) and Gram-negative *Salmonella enterica* serovar Typhimurium SL1344.

The antibacterial efficacy of hep-AgNPs/PU bandages samples was evaluated using the Kirby-Bauer disk diffusion method. An O/N LB culture was diluted 1:100 and incubated at 37 °C with aeration for ~1 h (equivalent to 0.5 McFarland standard, 1.5×10^8 CFU/ml). 100 μl aliquots were evenly spread onto Mueller-Hinton agar plates and allowed to dry. Circular fiber mat samples measuring approximately 16 mm in diameter were then positioned on the agar surface and allowed to incubate for 24 h at 37 °C. The zone of inhibition (in mm) was determined by subtracting the diameter of the fiber mat sample (D) from the diameter of the clear zone around the test specimen [T and dividing the result by 2 [(T − D) / 2]]. All experiments were conducted in triplicate.

3. Results and discussion

3.1. Synthesis and characterization of heparin capped silver nanoparticles

Scheme 1 shows the synthesis of heparin capped silver nanoparticles from cyst-AgNPs. Cyst-AgNPs were formulated from the method published by Olivia et al. [48] The obtained nanoparticles were characterized by Uv-vis spectroscopy (Fig. 1a). The strong absorbance at 430 nm is characteristic of surface plasmon resonance (SPR) of silver. The surface functionality of cyst-AgNPs was confirmed by FTIR spectroscopy that showed no free SH vibration (at 2596 cm^{-1} in Cyst) and a broad absorption at 3356 cm^{-1} attributed to the amine ($-NH_2$) functionality on cyst-AgNPs (Fig. S1). The size of the nanoparticles was measured by DLS spectroscopy and shows the overall hydrodynamic diameter at around 10–20 nm (Fig. 1b). The purified cyst-AgNPs were reacted with heparin polymer through amidation reaction condition using EDC as coupling reagent. Different ratios of heparin to AgNPs were initially tested to better understand the surface functionalization of AgNPs with heparin polymer. Each synthesis of cyst-AgNPs yields approximately 20 to 24 mg of nanoparticles and each nanoparticle has around 30 active sites of silver as depicted in *Olivia* et al. Considering this we initially used a very low ratio of cyst-AgNPs (1 eq) to heparin polymer (30 eq). However, due to the high concentration of heparin and very low amount of Ag nanoparticles, the white residue of heparin polymer was observed after the reaction. Following these, various lower concentrations of heparin polymer to Ag nanoparticles were assessed until the desired product was successfully synthesized. The two best and workable ratios of heparin to cyst-AgNPs were 1:1 and 2:1, monitored by UV–vis and FTIR. Heparin is a sulfated glycosaminoglycan mixture, which consists of unbranched polysaccharide chains, composed of 15 to 100 alternating monosaccharide units of L-iduronic acid and D-glucosamine, and has an active carboxylic acid group at every segment. Therefore, during the amidation reaction each acidic group is expected to react with $-NH_2$ of Ag nanoparticle which wraps its surface. Consequently, it is likely that the polymer wraps itself around the nanoparticles as it reacts.

The synthesized nanoparticles were characterized using various techniques. Surface plasmon resonance (SPR) of the resulting hep-AgNPs was examined via UV–vis spectroscopy (Fig. 1a). The spectra exhibit a strong absorption peak around 450 nm, indicative of the SPR phenomenon of silver (Ag) metal nanoparticles. DLS analysis (Fig. 1b) of hep-AgNPs (in red) revealed an increase in the overall hydrodynamic diameter to 70–90 nm, suggesting the successful conjugation of cyst-AgNPs with heparin. As heparin is a long-chain polymer with a higher molecular weight (15 kDa), its conjugation onto the surface of AgNPs is expected to increase the overall size and hydrodynamic diameter of the nanoparticles. Further characterization was performed using SEM microscopy to visualize the morphology and size of the particles. SEM images of the hep-AgNPs demonstrated monodisperse particles, with

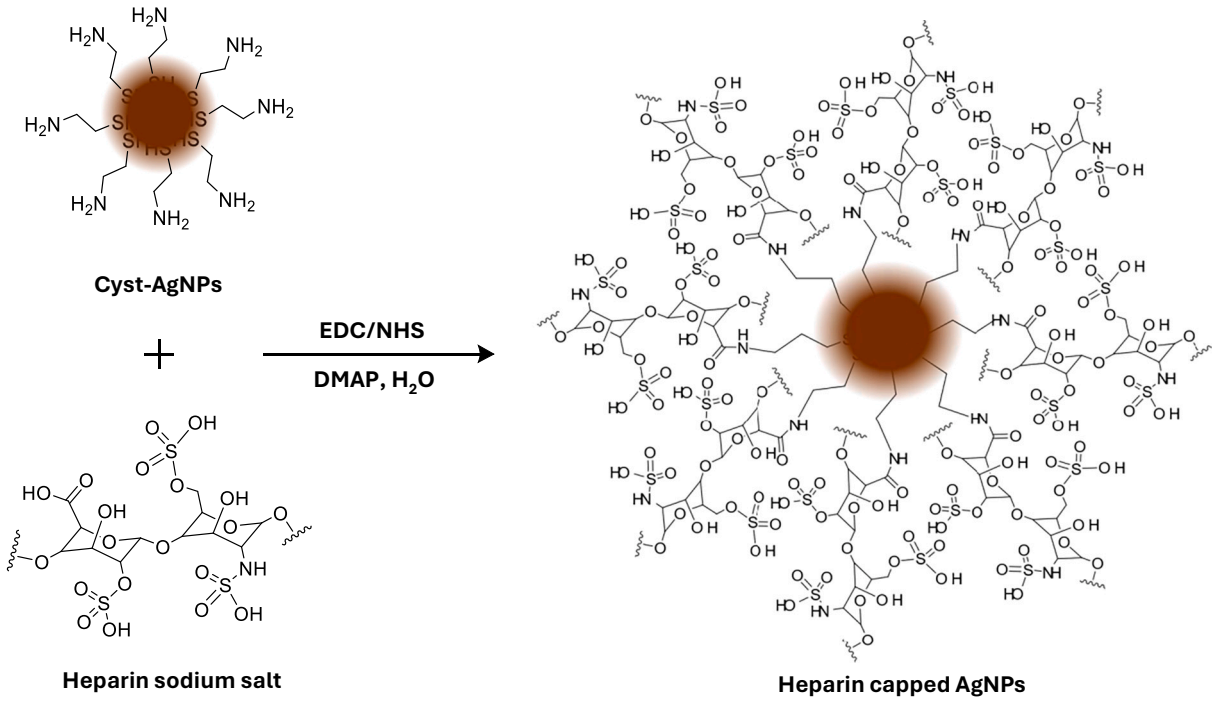

Scheme 1. Illustrates the process of synthesizing heparin-capped silver nanoparticles (AgNPs) using cysteamine-functionalized AgNPs (Cyst-AgNPs) as a starting material. The synthesis involves the amide bond formation between silver nanoparticles with heparin.

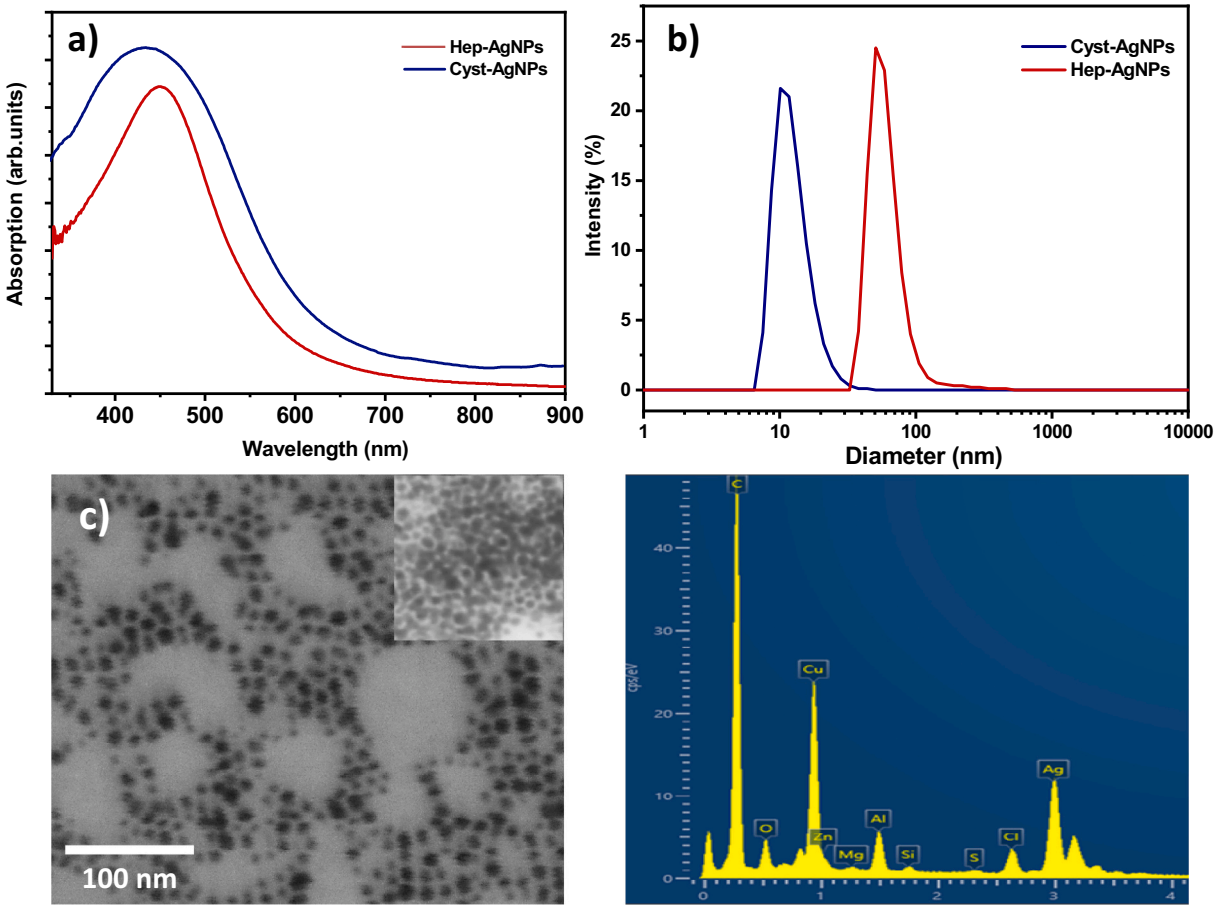

Fig. 1. a) showing the UV–Vis spectra of heparin-capped silver nanoparticles (hep-AgNPs) and cysteamine-functionalized silver nanoparticles (cyst-AgNPs) in water; b) highlighting the DLS spectra comparing hep-AgNPs with the starting material, cyst-AgNPs; c) illustrating the SEM images of hep-AgNPs, including an inset showing cyst-AgNPs; d) EDX spectra confirming the elemental analysis of hep-AgNPs.

most ranging from 11 ± 3 nm (Fig. 1c). The inset SEM image of the cyst-AgNPs in Fig. 1c illustrates the clustering or aggregated nature of the AgNPs. This is further evidence that the AgNPs are functionalized with heparin, as indicated by the increased distance between nanoparticles. The EDX analysis provides the insight into the elemental composition of the heparin capped silver nanoparticles. The EDX profile depicted in Fig. 1d, exhibits a prominent signal corresponding to the presence of Ag atoms. Additionally, strong peaks are observed for carbon (C) and oxygen (O), indicating the thick layer of heparin polymer on the surface of the Ag nanoparticles. The absorption peak at 3 keV is characteristic of silver nanocrystals, consistent with observations reported by Ravichandran et al. [52]. Table 1 is reporting the elemental composition of heparin capped silver nanoparticles.

Surface functionalization of hep-AgNPs was confirmed via FTIR spectroscopy (Fig. 2). The presence of the prominent peak at approximately 1695 cm^{-1}, corresponding to the C═O stretching vibration in the amide bond, signifies the successful coupling reaction between the carboxylic acid from heparin (1648 cm^{-1}) and the $-NH_2$ group from cyst-AgNPs. The peak at 1558 cm^{-1} corresponds to the N—H bending vibration, also indicating the formation of amide linkage. The symmetric and asymmetric stretching vibrations of sulfate ($-SO_4$) and sulfonate ($-SO_3$) groups from heparin are evident between 1200 and 1400 cm^{-1}. Peaks in the range of 989 cm^{-1} to 1187 cm^{-1} are attributed to the stretching vibration of the C-O-C bonds in the sugar ring of heparin. Broad peaks in the region of 3000–3700 cm^{-1} indicate the stretching vibration of the hydroxyl group (−OH) and possible residue of $-NH_2$ present in cyst-AgNPs. The peaks observed in the region of 2800–2900 cm^{-1} are attributed to the stretching and bending vibrations of the aliphatic −CHs present in both heparin and AgNPs. However, this characteristic is not as prominent in heparin alone.

3.2. Fabrication and morphology of nanofibers

To formulate the nanofibers wound dressings using the electrospinning technique, hep-AgNPs were mixed with the PU solution containing both DMF and THF. The choice of solvents and spinning parameters were optimized to achieve the desired outcome. Different concentrations of nanofibers bandages (hep-AgNPs in PU) were formulated to understand the toxicological threshold of the material in cells and effectiveness in bacterial culture.

Fig. 3 illustrates the surface morphologies of the wound healing bandages formulated with different concentrations of hep-AgNPs in PU polymer. Each formulated bandages were cut into a disk size of 16 mm in diameter. All the bandage samples containing hep-AgNPs in PU exhibit bead-free homogeneous fibers displaying smooth surfaces. As the concentration of hep-AgNPs in PU increases from 1 % to 10 % (*w*/w), there is a corresponding increase in the average fiber diameter. This phenomenon is attributed to the conductive nature of silver (Ag), which enhances the conductivity of the spinning solution and improves the electrospinning process. Consequently, this process yields smooth and thick nanofibrous mats. This increase in fiber diameter aligns with recent findings published by Miranda et al. [53] which report that when the total concentration reaches 10 % (*w*/w), the fluidity of the spinning liquid decreases, leading to needle plugging and hindering electrospinability. Therefore, a total solids content of 10 % was selected as the optimal concentration [53].

Table 1
Presenting the weight and atomic percentages of the prime elements detected in the samples, primarily silver (Ag) and carbon (C), for hep-AgNPs, Each sample was measured at various points to ensure accuracy and representativeness of the data.

Elements	C	O	Al	S	Cu	Ag
Atomic percentage (%)	69.33	10.68	1.35	4.47	4.97	9.31
Weight percentage (%)	33.31	6.83	1.46	5.60	12.64	40.16

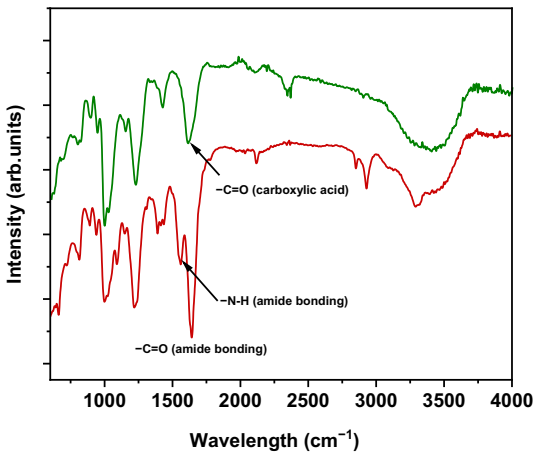

Fig. 2. FTIR spectra comparing heparin (green) with heparin-capped silver nanoparticles (red). This analysis highlights the functional groups present in both heparin and the modified nanoparticles, providing insights into the successful functionalization of heparin on the surface of silver nanoparticles.

3.3. Mechanical properties

Mechanical properties play a crucial role in the development of wound care bandages. These properties determine how the bandages interact with the wound site, how it conforms to the body's contours and how it provides support and protection during the healing process. The ability of the bandage to stretch and recover its original shape is essential for maintaining proper compression and ensuring a snug fit over the wound. The results of the mechanical test are presented in Table 2.

Fig. 4 presents the mechanical properties of polyurethane nanofibers wound dressings containing varying concentrations of hep-AgNPs. Stress-strain curves for different compositions (1 %, 3 %, 6 %, and 10 % hep-AgNPs/PU) illustrate changes in mechanical strength (Fig. 4A). Initially, tensile strength increased with 1 % hep-AgNPs/PU but decreased with further addition, while elongation at break initially increased but then decreased as hep-AgNPs concentration was raised. This trend suggests that higher nanoparticle loading enhances durability but reduces elasticity, possibly due to changes in porosity or interfacial bonding. The presence of hep-AgNPs initially improved both elongation at break and tensile strength (Fig. 4B and D), attributed to their reinforcement effect and enhanced interfacial bonding with the polymer matrix [54]. AgNPs, coated with heparin, facilitate hydrogen bonding within the PU matrix, contributing to mechanical enhancement [55]. Hep-AgNPs can also influence crystallinity and contribute to mechanical strength [56]. However, excessive hep-AgNPs led to agglomeration, weakening the material. Notably, Young's modulus decreases with hep-AgNP addition, reflecting reduced stiffness due to agglomeration [57]. Although hep-AgNP integration generally boosts mechanical properties, surpassing optimal concentrations negatively impacts elongation at break, tensile strength, and Young's modulus. Overall, the newly developed scaffolds exhibited adequate mechanical strength to safeguard burn wounds and prevent tearing during transport and storage [58]. The obtained values for tensile strength, elongation at break, and Young's modulus were similar to previously reported values for nanofiber wound dressings [59,60]. These findings align with the reported range of tensile strength (0.8 to 18.0 MPa) considered suitable for skin cell culture [61].

3.4. Water absorption and water vapor transmission rates

Water absorption and transmission rates are critical factors to consider in wound dressing design as they directly affect wound healing outcomes, patient comfort, and overall wound care management.

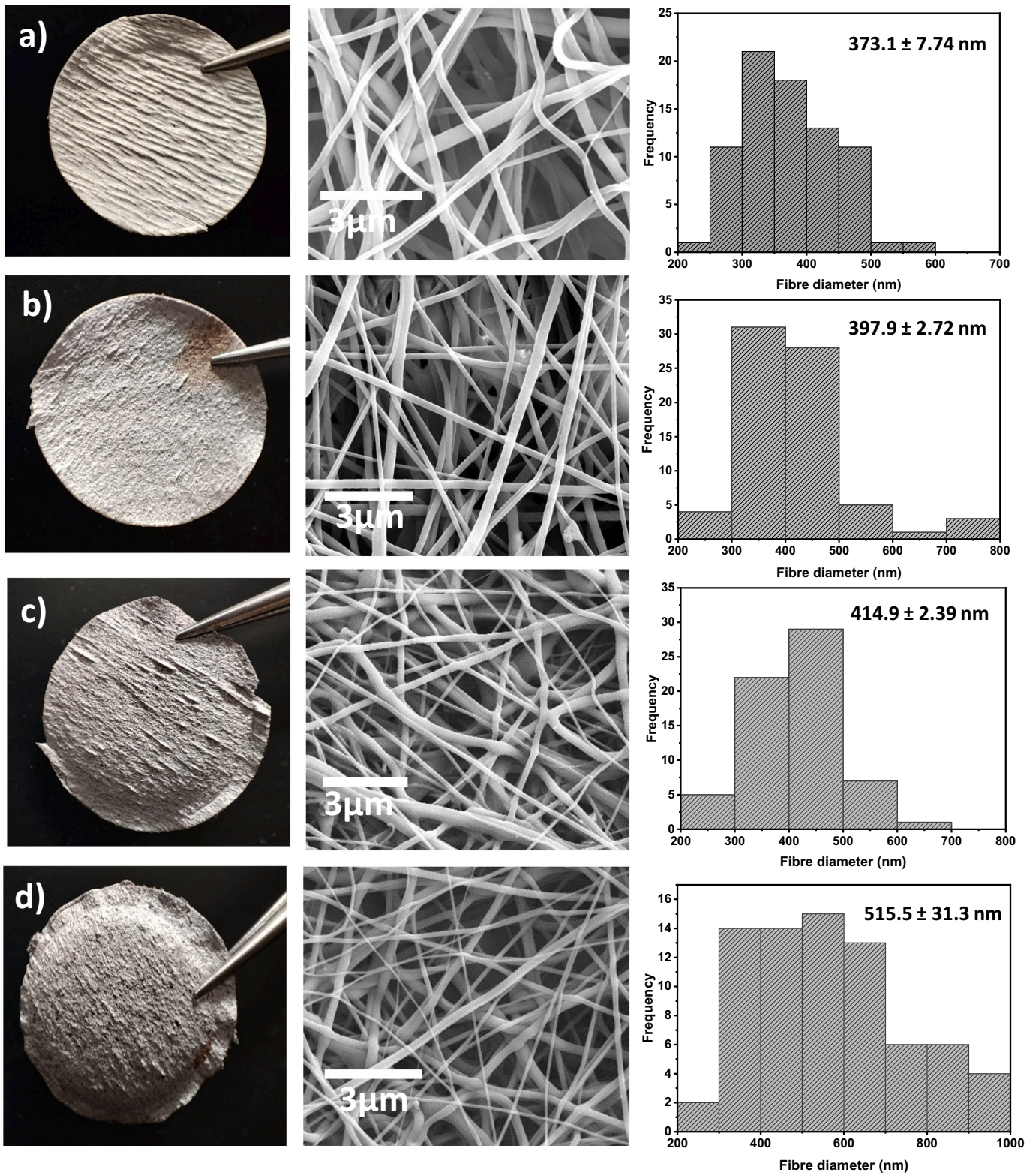

Fig. 3. Showing the surface morphology of nanofiber bandages (16 mm) visualized through SEM images and a bar chart of fiber diameters for various compositions: a) 1 % hep-AgNPs/PU, b) 3 % hep-AgNPs/PU, c) 6 % hep-AgNPs/PU, and d) 10 % hep-AgNPs/PU. This analysis highlights the impact of hep-AgNPs concentration on the fiber structure and diameter.

Dressings with proper moisture management properties create a conducive healing environment, facilitate wound healing, and decrease the risk of complications [62]. Fig. 5 illustrates the wound exudate absorption capacity of the new nanofiber wound dressings by evaluating their water absorption rates.

The fluid absorbency, retention, and handling capacity of the nanofibrous wound dressings were assessed using the standard EN 13726-1 test. Fig. 5a illustrates that the water absorption capacity of the nanofiber wound dressings was significantly higher compared to the pure PU-based wound dressing. The fluid absorbency is influenced by

Table 2
Showing the mechanical properties of nanofibers including tensile strength, elongation at break, Young's modulus, and thickness for different compositions: pure polyurethane (PU) and PU incorporated with varying concentrations of heparin-capped silver nanoparticles (hep-AgNPs). The data highlights the effects of hep-AgNPs on the mechanical performance of the nanofibers, showing variations in tensile strength and elongation at break with increasing nanoparticle concentration.

Nanofibers	Tensile strength (MPa)	Elongation at break (%)	Young's modulus (MPa)	Thickness (μm)
PU	7.13	122.24	5.83	0.20
1 % hep-AgNPs/PU	11.9	239.02	4.97	0.30
3 % hep-AgNPs/PU	7.03	191.92	3.66	0.33
6 % hep-AgNPs/PU	5.12	159.04	3.21	0.30
10 % hep-AgNPs/PU	4.83	158.27	3.05	0.25

both the chemical and physical properties of the material. Chemically, the PU nanofibers are infused with heparin-functionalized AgNPs, leveraging heparin's high hydrophilicity to enhance fluid absorption. Physically, the dressings consist of fine fibers formed through electrospinning, resulting in numerous pores that can trap water molecules due to their structural properties. However, increasing the concentration of hep-AgNPs further in the PU nanofibers leads to a decrease in water absorption capacity. This additional increase of concentration alters the structure of PU fibers, reducing fiber porosity, introducing barriers to water diffusion, and increasing hydrophobicity, resulting in decreased water absorbency. The wound dressing's high fluid retention capacity refers to its ability to retain absorbed fluid within the structure, even under pressure. This helps to keep contamination away, prevent maceration and leakage, leading to a reduction in the frequency of dressing changes.

Fig. 5a demonstrates the high fluid absorbance and retention value of the nanofibers wound dressings making them suitable for wound healing applications [63,64]. Fig. 5b shows the water vapor transmission rates (WVTR) of the nanofibers wound dressings. WVTR is a critical parameter in wound healing management. A wound dressing with appropriate WVTR allows excess moisture, such as wound exudate, to evaporate from the wound surface while preventing excessive moisture build up

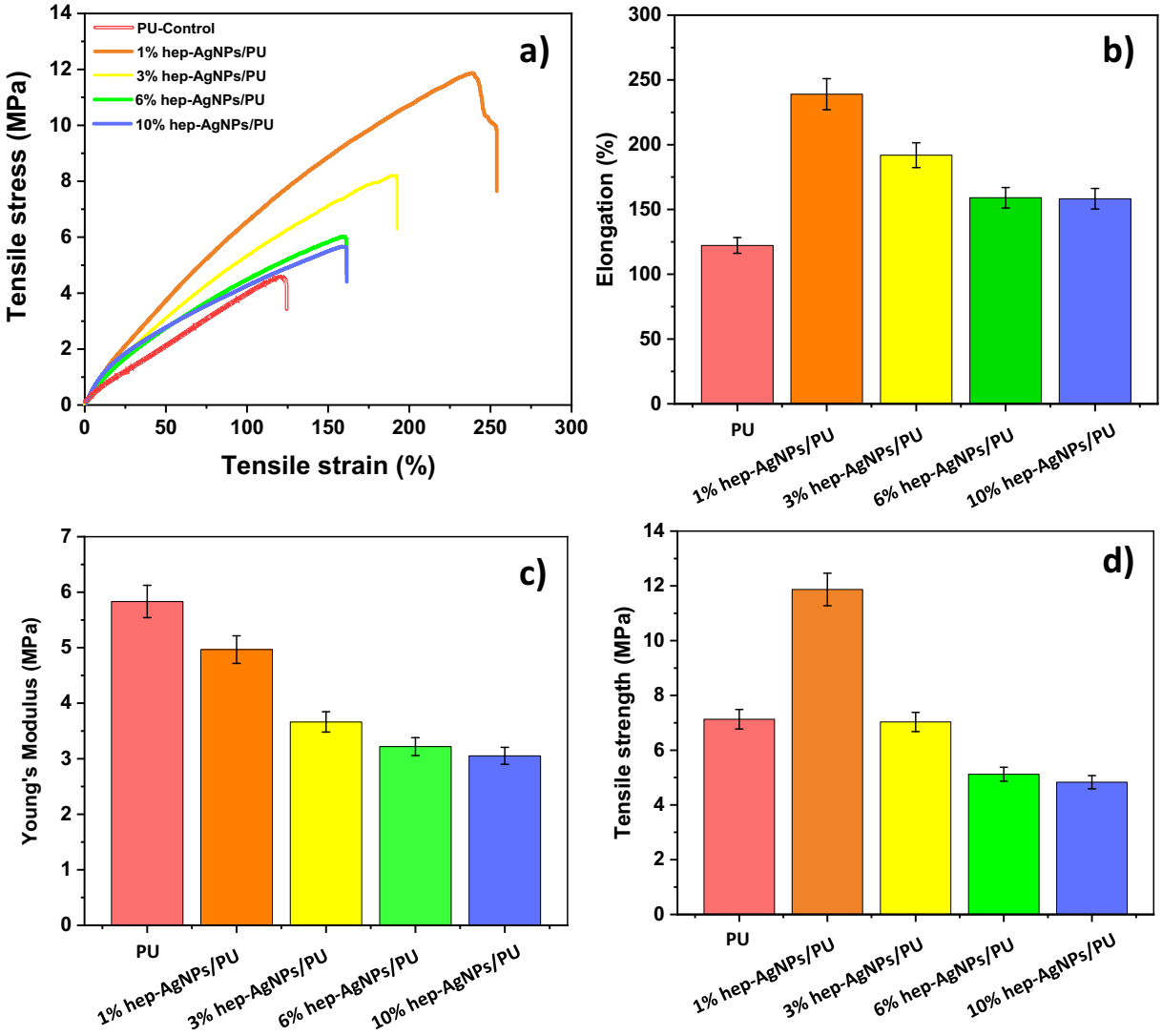

Fig. 4. Mechanical properties of polyurethane (PU) nanofibers infused with heparin-capped silver nanoparticles (hep-AgNPs) at various concentrations. The figure presents (A) strain-stress curves, (B) ultimate strain, (C) Young's modulus, and (D) tensile strength, with data expressed as mean ± SD ($n > 4$). This analysis illustrates how varying concentrations of hep-AgNPs influence the mechanical performance of the wound dressing.

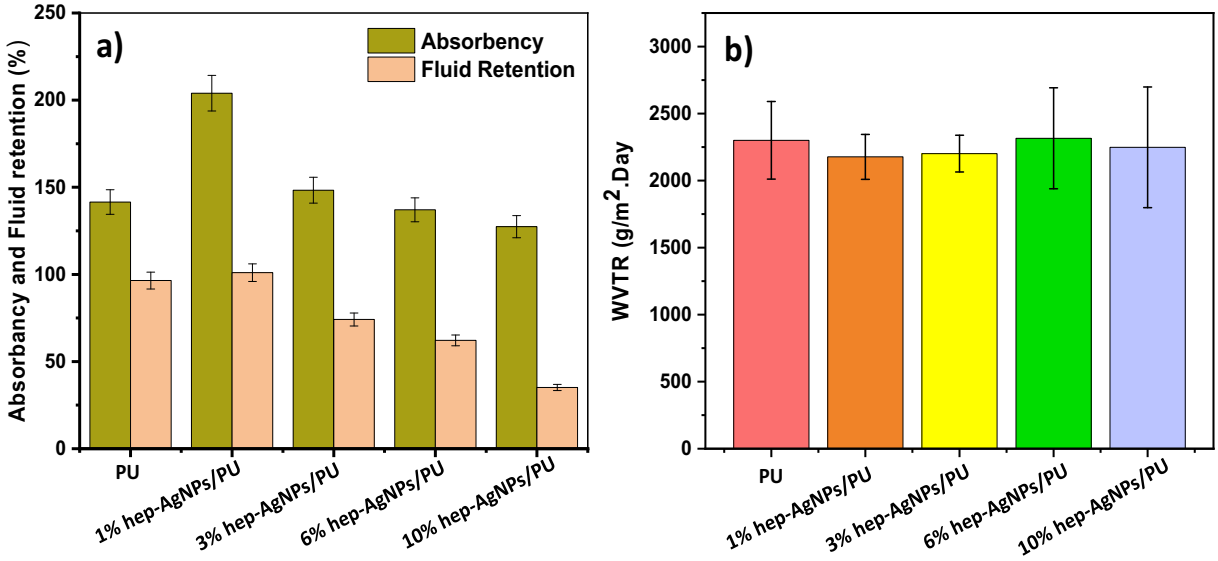

Fig. 5. Showing the fluid absorbance and retention (a) and water vapor transmission rate (b) of nanofiber wound dressings. Data represented as mean ± SD ($n > 3$), illustrating the performance characteristics of the dressings in terms of fluid management and breathability.

which can lead to maceration and maintain the wound clean and hygienic, contributing to patient's comfort and reducing the risk of further infection [65]. Our nanofibers wound dressings exhibits excellent WVTR. Interestingly even pure PU shows high WVTR (2312.82 g $^{-2}$/day $^{-1}$) compared with the hep-AgNPs loaded wound dressings. It has been suggested that the ideal WVTR values should be within the range of 2000–2500 g $^{-2}$/day $^{-1}$ [66]. All the nanofibers wound dressings loaded with various concentrations of hep-AgNPs showed WVTR values close to the desired range. Therefore, it is expected that the formulated wound dressing material is quite suitable for wound care applications.

3.5. Water contact angle analysis

Since the nanofibers bandages are intended for wound healing applications and will come into contact with skin, water, and bodily fluids, it is crucial to analyze their wettability. Fig. 6 represents images from the wettability analysis of the electrospun PU nanofibers bandages containing various concentrations of hep-AgNPs, measured using a water contact angle at different time points. The PU nanofibers (without hep-AgNPs) displayed hydrophobic characteristics initially at 0 s with a contact angle of 118.7°. After the addition of hep-AgNPs the water contact angle of the formulated bandages were expected to decrease because of the hydrophilic nature of hep-AgNPs. However the water contact angle displayed was higher than that of PU. This phenomenon was probably due to the surface roughness of electrospun nanofibers which often have high surface area-to-volume ratio and can possess surface irregularities or roughness at the nanoscale. These rough surfaces can trap air pockets, preventing water from wetting the surface fully and leading to a higher contact angle. From Figs. 6A and B it can be seen that the water contact angle decreased by up to 60° at 120 s and this reflects the hydrophilic nature of the nanofibers bandages. The ideal water contact angle for wound healing bandages typically falls within the range of 40° to 90°. This range indicates moderate to high hydrophilicity, facilitating proper moisture management and promoting an optimal wound healing environment [67,68].

3.6. Release study of Ag from nanofibers wound dressings

The controlled release of drugs from wound healing bandages plays a crucial role in wound management by facilitating localized treatment, enhancing wound healing, controlling infections, managing pain, reducing treatment frequency, customizing therapy, and minimizing systematic side effects. This approach improves patients' outcomes and overall quality of care in wound management. Fig. 7 displays the cumulative silver release profile of different concentrations of hep-AgNPs incorporated into PU nanofibers bandages. The 1 % hep-AgNPs/PU (0.3 % Ag) dressing show a biphasic release of silver profile, demonstrating the fast release of silver (up to 40 %) within 1 day, followed by slow diffusion-controlled release within 7 days. The initial fast release was also seen at higher concentrations however the percentage of silver release was much lower than that of the 1 % hep-AgNPs/PU dressings. The initial fast release of silver is related to the hydrophilic nature of heparin present on the surface of the Ag nanoparticles. The hep-AgNPs present on the surface of the fibers are able to diffuse and release faster than those present inside the fibers. The second slower release rate could be attributed to the slower diffusion of hep-AgNPs from inside the fibers from the non-degradable polyurethane matrix before diffusion into the bulk. As the drug loading increased from 1 % to 10 %, the elution of hep-AgNPs decreased, likely due to the hindered release or extravasation of hep-AgNPs from the fibers. As seen earlier, the increased concentration of hep-AgNPs also caused an increase in the average diameter of the nanofibers (Fig. 3); this resulted in decreasing the available surface area to solution ratio and consequently influenced the swelling ratio of the nanofibers. The beneficial desired sustained Ag release indicated that the hep-AgNPs embedded PU bandages are suitable for a long-term antimicrobial application during the wound healing process.

3.7. Cell viability assay

Wound healing bandages often incorporate bioactive agents such as growth factors, antimicrobial agents, or anti-inflammatory compounds to promote wound healing. In vitro toxicity testing helps evaluate the cytotoxicity of these bioactive agents to ensure they are effective in promoting wound healing without causing harm to cells or tissues. The in vitro toxicity effect of our nanofiber bandages was investigated on HaCat and L929 cell lines (Fig. 8a and b). The formulated wound healing bandages were compared with commercial bandages containing silver. Interestingly, our nanofiber wound healing bandages exhibited excellent biocompatibility compared to commercial bandages. The formulated hep-AgNPs/PU wound healing bandages did not show any toxicity at an initial concentration of 1 % hep-AgNPs/PU. However, as the concentration of silver nanoparticles increased from 3 % hep-AgNPs to 10 % hep-AgNPs, a minimal inhibitory effect on keratinocytes and fibroblasts

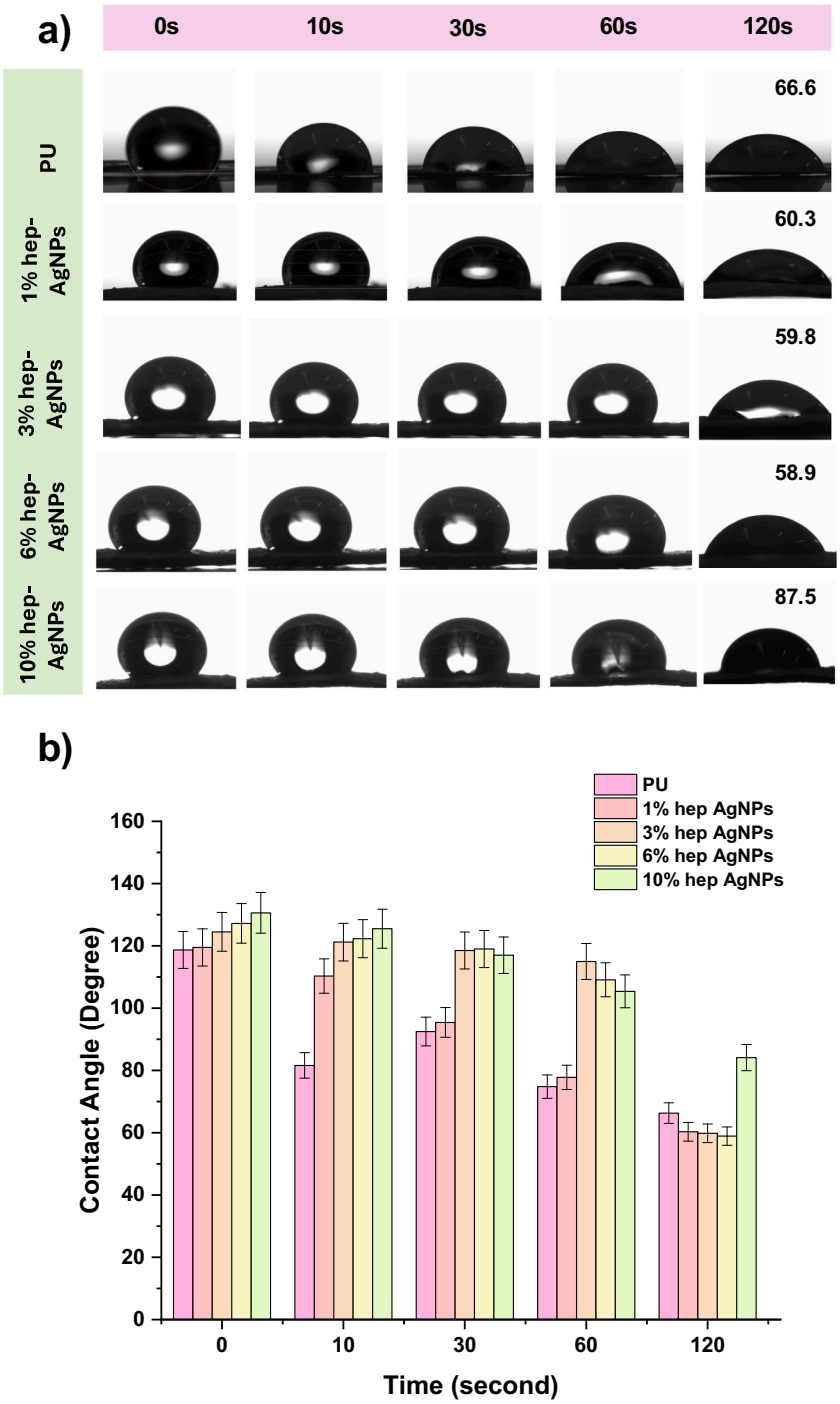

Fig. 6. a) Water contact angle of electrospun PU nanofiber wound healing bandages infused with hep-AgNPs. b) Graphical representation of the water contact angle data. Values are expressed as mean ± SD ($n \geq 1.5$), highlighting the hydrophilicity of the nanofibers.

was observed. In contrast, the commercial bandages showed high toxicity at 24 h, evidenced by growth inhibition of keratinocytes and fibroblasts. The formulated hep-AgNPs embedded PU bandages were shown to promote cell growth even at high concentrations, possibly due to the angiogenic properties of heparin promoting cell growth.

3.8. Wound healing assay

The scratch assay for wound healing, initially introduced by Gabbiani et al. [69] in 1984, offers a straightforward method for assessing fibroblast and keratinocytes migration in vitro, serving as a dependable model for skin cell movement. Fibroblast and keratinocyte migration plays a pivotal role in the wound healing process, encompassing crucial functions such as fibrin clot breakdown, synthesis of new extracellular matrix and collagen, and wound contraction. Consequently, investigating the migration of crucial cells in response to various stimuli can aid in identifying targeted therapies for enhancing wound healing efficacy.

The effect of the various nanofibers bandages on HaCat cell lines was evaluated. Fig. 9 shows the efficacy of the formulated nanofibers bandages when compared with blank polyurethane and commercial bandages to evaluate the efficacy. As compared with control and blank PU,

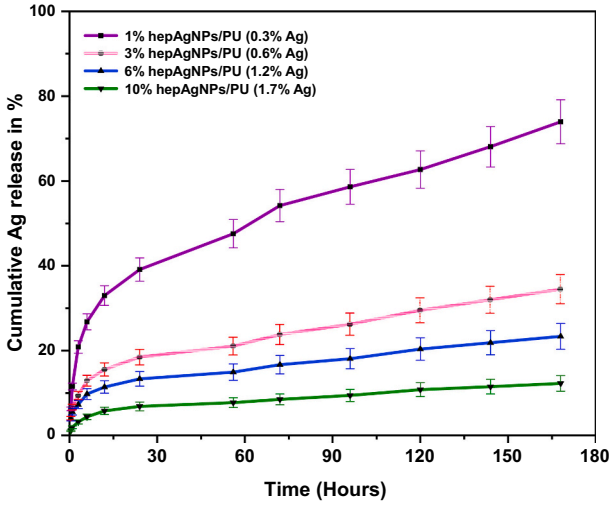

Fig. 7. Cumulative release profile of silver (Ag) from hep-AgNPs embedded PU nanofiber wound dressings in phosphate-buffered saline (PBS). The total percentage of silver in each sample is shown in the legend. Data are presented as mean ± SD ($n \leq 2$), highlighting the release behavior over time.

the nanofibers bandages are shown to be quite effective for keratinocyte migration. After 24 h, the nanofibers bandages visibly promoted cell proliferation as well as keratinocyte migration at the in vitro wound healing site. The effective wound closure can be seen within 48 h, whereas the control and blank PU show slower migration of keratinocytes and consequently slower wound closure. The faster wound healing and cell proliferation ability of various nanofibers wound healing bandages is attributed to the superiority of heparin. Heparin is well known for its potential effects on keratinocyte migration, which is a critical aspect of wound healing, particularly in re-epithelialization, where keratinocytes migrate to cover the wound bed [46]. Heparin boosts EGF and FGF activity, vital for keratinocyte migration and proliferation [70]. Its anti-inflammatory properties create a favorable environment for keratinocyte migration. Heparin aids ECM remodeling, promoting cell adhesion and guiding keratinocyte movement [71]. Well known for its angiogenesis promotion, heparin indirectly supports keratinocyte migration by fostering new blood vessel formation [72]. Heparin regulates the wound microenvironment, impacting cell adhesion and growth factor availability, influencing keratinocyte migration dynamics [73]. Accordingly, heparin demonstrates its excellent ability for promoting the wound healing process and thereby avoiding the occurrence of chronic inflammation. The obtained result indicates that AgNPs functionalized with heparin exhibit potential for future use in skin engineering and critical wound repair applications.

3.9. Antimicrobial activity

The antibacterial activity of the nanofibers bandages was evaluated against two diverse bacterial species, Gram-positive *Staphylococcus aureus* and Gram-negative *Salmonella Typhimurium* with differing cellular architecture and metal resistance mechanisms. The antibacterial activity of the PU nanofibers bandages infused with hep-AgNPs was compared with that of commercial bandages and the results depicted in Fig. 10 using the Kirby-Bauer disk diffusion method. Blank nanofiber PU bandages (without hep-AgNPs) did not affect bacterial growth, however the samples containing various concentrations of hep-AgNPs displayed zones of inhibition from ~0.2 mm to 5 mm for *S. typhimurium* and *S. aureus*. As the concentration of hep-AgNPs in the nanofibers bandages increases, the zone of inhibition also increases. Interestingly, the commercial samples A and B, were found to be less effective when compared with the formulated hep-AgNPs/PU nanofibers bandages samples. The antibacterial activity of silver nanoparticles has been well described [15] and involves the disruption of bacterial membranes and inhibition of biofilm formation, making them effective against a wide range of bacteria, including multidrug-resistant strains [18].

While primarily recognized for its anticoagulant effect, heparin also demonstrates antibacterial properties. It is reported that heparin disrupts bacterial cell membranes by interacting with the lipopolysaccharides (LPS) in Gram-negative bacteria or peptidoglycans in Gram-positive bacteria [44]. This disruption can lead to leakage of cellular contents and ultimately causes bacterial death. Heparin has also been shown to inhibit the formation of bacterial biofilms, by interfering with the adherence of bacteria to surfaces and with the production of the biofilm matrix [45]. Moreover it is reported that heparin may prevent bacteria from adhering to host cells or tissues by competing for binding sites on the bacterial surface [74]. This interference with bacterial adhesion can impede the establishment of infection and facilitate bacterial clearance by the immune system. Some studies suggest that heparin possesses direct bactericidal activity against certain bacterial strains. The exact mechanism underlying this activity is not well-defined

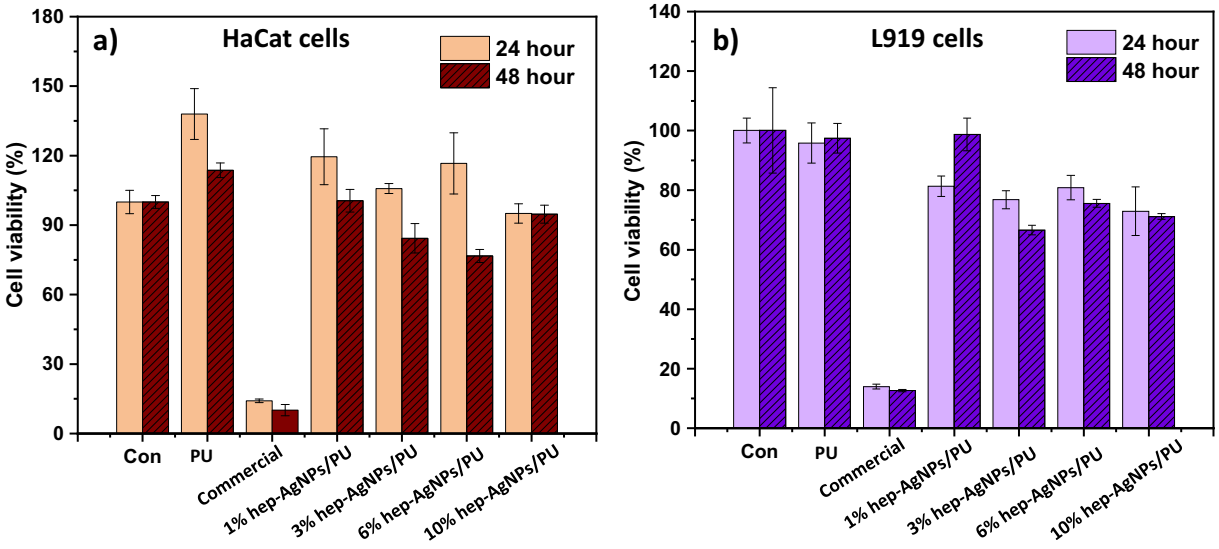

Fig. 8. Cell proliferation assay showing the effects of various concentrations of wound healing bandages on (a) HaCat and (b) L929 cell lines. Data are presented as mean ± SD ($n \geq 3$), demonstrating the impact of the bandages on cell growth. There are significant differences between the two cell lines, with p-value of <0.001.

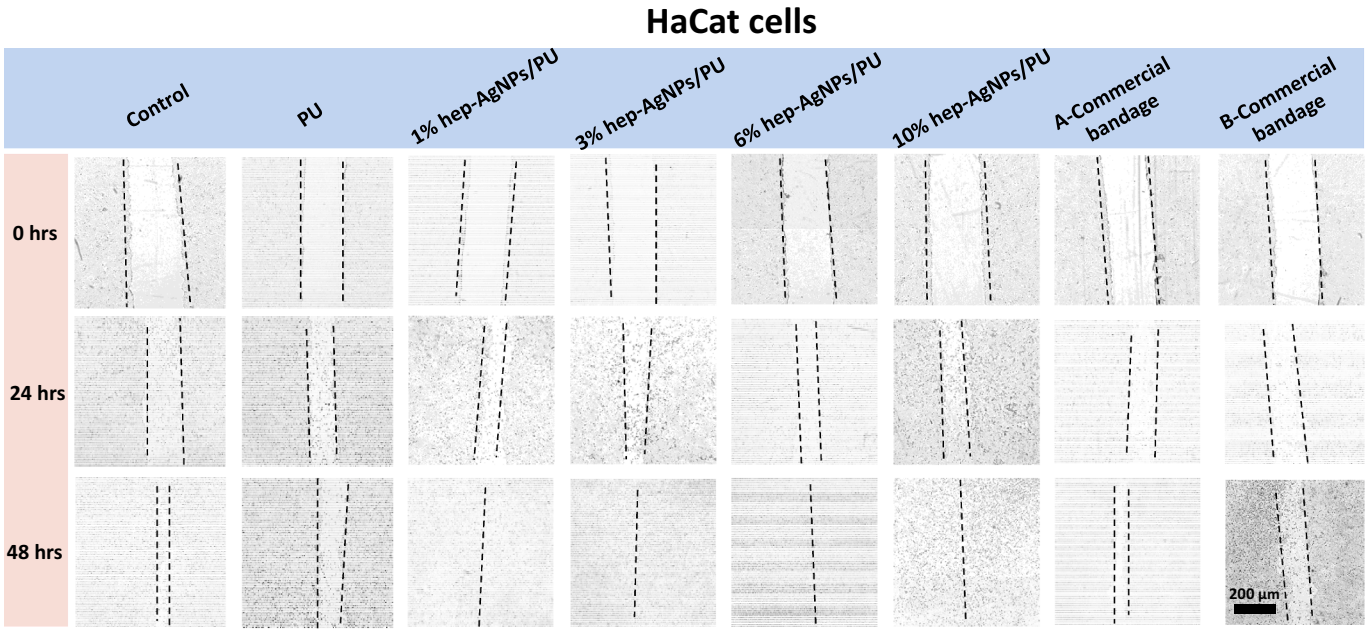

Fig. 9. Cell migration and proliferation assay of various concentrations of hep-AgNPs wound healing bandages on HaCat cell lines. This figure illustrates how different concentrations influence both the migration and proliferation of the cells, highlighting the potential effectiveness of the bandages in promoting wound healing.

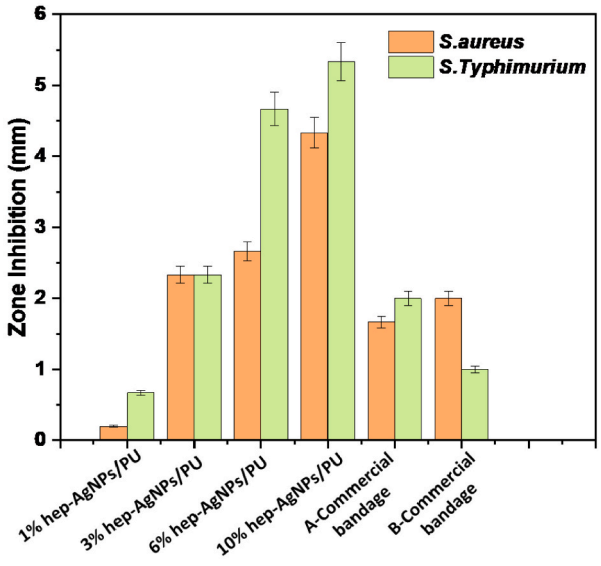

Fig. 10. Antimicrobial activity of nanofiber bandages infused with varying concentrations of hep-AgNPs against *Staphylococcus aureus* and *Salmonella Typhimurium*. Bacterial cultures were grown on Mueller-Hinton agar, and the zones of inhibition were measured following exposure to the hep-AgNPs bandage using the Kirby-Bauer method. Data represent the means of three separate experiments performed in triplicate, with error bars indicating mean ± SD ($n \geq 1$).

but may involve disruption of bacterial cell wall integrity or interference with essential bacterial metabolic processes. Overall, while the precise antibacterial mechanism of heparin remains to be fully elucidated, its multifaceted actions suggest potential therapeutic applications beyond its well-established anticoagulant effect.

4. Conclusions

In this study, heparin-capped silver nanoparticles (hep-AgNPs) were synthesized and integrated into polyurethane (PU) nanofibers, presenting a novel approach with significant implications for wound healing applications. The incorporation of hep-AgNPs into PU fibers through electrospinning not only improved the mechanical strength and flexibility of the wound dressings but also enhanced their antibacterial efficacy, biocompatibility, and overall wound healing potential. The nanofiber bandages displayed a slow and sustained release of hep-AgNPs, leading to prolonged therapeutic effects, reduced dosage frequency, and minimized systemic absorption, all contributing to improved patient comfort and optimized wound care outcomes. The nanofibrous dressings exhibited excellent antibacterial activity against both *Staphylococcus aureus* and *Salmonella Typhimurium*, surpassing commercial wound healing bandages while maintaining non-toxic properties in keratinocytes and fibroblasts. This positions the hep-AgNPs/PU nanofibers as a promising candidate for advanced wound healing, especially in treating chronic and infected wounds. Moreover, the study delved into the broader biomedical potential of heparin beyond its traditional anticoagulant role. Heparin's ability to modulate inflammation and interact with multiple disease-related proteins underscores its potential in various therapeutic areas, including cancer, infections, and neurodegenerative diseases. However, challenges such as managing its potent anticoagulant effects, standardizing dosage, and addressing safety concerns remain critical for its broader clinical application. Future research should focus on understanding the precise mechanisms of hep-AgNPs in wound healing and exploring the development of customized heparin derivatives with enhanced therapeutic benefits, potentially paving the way for new, more effective biomedical applications.

CRediT authorship contribution statement

Jayshree H. Ahire: Writing – review & editing, Writing – original draft, Visualization, Validation, Supervision, Software, Resources, Project administration, Methodology, Investigation, Funding acquisition, Formal analysis, Data curation, Conceptualization. **Qi Wang:** Writing – review & editing, Validation, Methodology, Investigation. **Gary Rowley:** Writing – review & editing, Methodology, Investigation. **Isabelle Chambrier:** Writing – review & editing, Validation. **Jason C.**

Crack: Writing – review & editing, Methodology. **Yongping Bao:** Writing – review & editing, Supervision, Resources. **Yimin Chao:** Supervision, Resources.

Declaration of competing interest

The authors declare that they have no known competing financial interests or personal relationships that could have appeared to influence the work reported in this paper.

Acknowledgements

I would like to express my sincere appreciation for the funding provided by the Daphne Jackson Trust, UK, The Royal Society of Chemistry (RSC), and University of East Anglia (UEA), without which this research would not have been possible. I am grateful to Prof Dmitry Pshezhetskiy for his invaluable discussions and advice. Special thanks to Professor Nick E. Le Brun for his support, guidance. Thanks to Dr. Linda Troeberg from UEA for generously supplying the L929 cells, and to Dr. Chris Morris from UCL for providing the HaCat cells.

Appendix A. Supplementary data

Supplementary data to this article can be found online at https://doi.org/10.1016/j.ijbiomac.2024.136557.

Data availability

Data will be made available on request.

References

[1] P. Dadgostar, Antimicrobial resistance: implications and costs, Infect. Drug Resist. 12 (2019) 3903–3910, https://doi.org/10.2147/IDR.S234610.
[2] G.R. Aguilar, L.R. Swetschinski, N.D. Weaver, K.S. Ikuta, T. Mestrovic, A.P. Gray, et al., The burden of antimicrobial resistance in the Americas in 2019: a cross-country systematic analysis, Lancet Reg. Health - Am. (2023) 25, https://doi.org/10.1016/j.lana.2023.100561.
[3] A. Kramer, A. Maassen, Wound dressings from a hygienic point of view using the example of sorbion sachet S, GMS HIC 4 (2) (2009) 2, https://doi.org/10.3205/dgkh000136.
[4] E.A. Grice, J.A. Segre, The skin microbiome, Nat. Rev. Microbiol. 9 (4) (2011) 244–534, https://doi.org/10.1038/nrmicro2537.
[5] F. Yousefian, R. Hesari, T. Jensen, S. Obagi, A. Rgeai, G. Damiani, et al., Antimicrobial wound dressings: a concise review for clinicians, Antibiotics (Basel) 12 (9) (2023) 9, https://doi.org/10.3390/antibiotics12091434.
[6] Y. He, H. Li, X. Fei, L. Peng, Carboxymethyl cellulose/cellulose nanocrystals immobilized silver nanoparticles as an effective coating to improve barrier and antibacterial properties of paper for food packaging applications, Carbohydr. Polym. 252 (2021) 117156, https://doi.org/10.1016/j.carbpol.2020.117156.
[7] S.M. Mousavi, S.A. Hashemi, Y. Ghasemi, A. Atapour, A.M. Amani, A. Savar Dashtaki, et al., Green synthesis of silver nanoparticles toward bio and medical applications: review study, Artif. Cells Nanomed. Biotechnol. 46 (sup3) (2018), https://doi.org/10.1080/21691401.2018.1517769 (S855-S72sup3).
[8] A. Partovi, M. Khedrinia, S. Arjmand, S.O. Ranaei Siadat, Electrospun nanofibrous wound dressings with enhanced efficiency through carbon quantum dots and citrate incorporation, Sci. Rep. 14 (1) (2024) 192561, https://doi.org/10.1038/s41598-024-70295-9.
[9] A.K. Bhardwaj, S. Sundaram, K.K. Yadav, A.L. Srivastav, An overview of silver nano-particles as promising materials for water disinfection, Environ. Sci. Technol. 23 (2021) 101721, https://doi.org/10.1016/j.eti.2021.101721.
[10] E.O. Mikhailova, Silver nanoparticles: mechanism of action and probable bio-application, J. Funct. Biomater. 11 (4) (2020) 4, https://doi.org/10.3390/jfb11040084.
[11] W.T.J. Ong, K.L. Nyam, Evaluation of silver nanoparticles in cosmeceutical and potential biosafety complications, Saudi J. Biol. Sci. 29 (4) (2022) 2085–2944, https://doi.org/10.1016/j.sjbs.2022.01.035.
[12] M. Rybka, Ł. Mazurek, M. Konop, Beneficial effect of wound dressings containing silver and silver nanoparticles in wound healing-from experimental studies to clinical practice, Life (Basel) 13 (1) (2022) 1, https://doi.org/10.3390/life13010069.
[13] A. Meher, A. Tandi, S. Moharana, S. Chakroborty, S.S. Mohapatra, A. Mondal, et al., Silver nanoparticle for biomedical applications: a review, Hybrid Adv. 6 (2024) 100184, https://doi.org/10.1016/j.hybadv.2024.100184.
[14] H.H. Lara, E.N. Garza-Treviño, L. Ixtepan-Turrent, D.K. Singh, Silver nanoparticles are broad-spectrum bactericidal and virucidal compounds, J. Nanobiotechnol. 9 (1) (2011) 301, https://doi.org/10.1186/1477-3155-9-30.
[15] W.K. Jung, H.C. Koo, K.W. Kim, S. Shin, S.H. Kim, Y.H. Park, Antibacterial activity and mechanism of action of the silver ion in *Staphylococcus aureus* and *Escherichia coli*, Appl. Environ. Microbiol. 74 (7) (2008) 2171–2187, https://doi.org/10.1128/AEM.02001-07.
[16] S.W. Kim, J.H. Jung, K. Lamsal, Y.S. Kim, J.S. Min, Y.S. Lee, Antifungal effects of silver nanoparticles (AgNPs) against various plant pathogenic fungi, Mycobiology 40 (1) (2012) 53–81, https://doi.org/10.5941/MYCO.2012.40.1.053.
[17] X.-F. Zhang, Z.-G. Liu, W. Shen, S. Gurunathan, Silver nanoparticles: synthesis, characterization, properties, applications, and therapeutic approaches, Int. J. Mol. Sci. 17 (9) (2016) 15349, https://doi.org/10.3390/ijms17091534.
[18] M. Szymczak, J.A. Pankowski, A. Kwiatek, B. Grygorcewicz, J. Karczewska-Golec, K. Sadowska, et al., An effective antibiofilm strategy based on bacteriophages armed with silver nanoparticles, Sci. Rep. 14 (1) (2024) 90881, https://doi.org/10.1038/s41598-024-59866-y.
[19] C. He, X. Liu, Z. Zhou, N. Liu, X. Ning, Y. Miao, et al., Harnessing biocompatible nanofibers and silver nanoparticles for wound healing: sandwich wound dressing versus commercial silver sulfadiazine dressing, Mater. Sci. Eng. C 128 (2021) 112342, https://doi.org/10.1016/j.msec.2021.112342.
[20] C. Liu, Y. Zhu, X. Lun, H. Sheng, A. Yan, Effects of wound dressing based on the combination of silver@curcumin nanoparticles and electrospun chitosan nanofibers on wound healing, Bioengineered 13 (2) (2022) 4328–4392, https://doi.org/10.1080/21655979.2022.2031415.
[21] Z.B. Nqakala, N.R.S. Sibuyi, A.O. Fadaka, M. Meyer, M.O. Onani, A.M. Madiehe, Advances in nanotechnology towards development of silver nanoparticle-based wound-healing agents, Int. J. Mol. Sci. 22 (20) (2021) 1127220, https://doi.org/10.3390/ijms222011272.
[22] P.J. Babu, A. Tirkey, A.A. Paul, K. Kristollari, J. Barman, K. Panda, et al., Advances in nano silver-based biomaterials and their biomedical applications, Eng. Regen. 5 (3) (2024) 326–413, https://doi.org/10.1016/j.engreg.2024.07.001.
[23] R.C.d. Souza, L.U. Haberbeck, H.G. Riella, D.H.B. Ribeiro, B.A.M. Carciofi, Antibacterial activity of zinc oxide nanoparticles synthesized by solochemical process, Braz. J. Chem. Eng. 36 (2019), https://doi.org/10.1590/0104-6632.20190362s20180027.
[24] M.S. Waghmode, A.B. Gunjal, J.A. Mulla, N.N. Patil, N.N. Nawani, Studies on the titanium dioxide nanoparticles: biosynthesis, applications and remediation, SN Appl. Sci. 1 (4) (2019) 3104, https://doi.org/10.1007/s42452-019-0337-3.
[25] F.M. Husain, F.A. Qais, I. Ahmad, M.J. Hakeem, M.H. Baig, J. Masood Khan, et al., Biosynthesized zinc oxide nanoparticles disrupt established biofilms of pathogenic bacteria, Appl. Sci. 12 (2) (2022) 7102, https://doi.org/10.3390/app12020710.
[26] P. Singh Jassal, D. Kaur, R. Prasad, J. Singh, Green synthesis of titanium dioxide nanoparticles: development and applications, J. Agric. Food Res. 10 (2022) 100361, https://doi.org/10.1016/j.jafr.2022.100361.
[27] J. Nandhini, E. Karthikeyan, S. Rajeshkumar, Nanomaterials for wound healing: current status and futuristic frontier, Biomed. Tech. 6 (2024) 26–45, https://doi.org/10.1016/j.bmt.2023.10.001.
[28] P.T.S. Kumar, V.K. Lakshmanan, R. Biswas, S.V. Nair, R. Jayakumar, Synthesis and biological evaluation of chitin hydrogel/nano ZnO composite bandage as antibacterial wound dressing, J. Biomed. Nanotechnol. 15 (9) (2019), https://doi.org/10.1166/jbn.2019.2824 (1994-59).
[29] A. Yari, H. Yeganeh, H. Bakhshi, R. Gharibi, Preparation and characterization of novel antibacterial castor oil-based polyurethane membranes for wound dressing application, J. Biomed. Mater. Res. A 102 (1) (2014) 84–961, https://doi.org/10.1002/jbm.a.34672.
[30] M. Moghanizadeh-Ashkezari, P. Shokrollahi, M. Zandi, F. Shokrolahi, Polyurethanes with separately tunable biodegradation behavior and mechanical properties for tissue engineering, Polym. Adv. Technol. 29 (1) (2018), https://doi.org/10.1002/pat.4160 (528-401).
[31] H. Yeganeh, M.M. Lakouraj, S. Jamshidi, Synthesis and characterization of novel biodegradable epoxy-modified polyurethane elastomers, J. Polym. Sci. A Polym. Chem. 43 (14) (2005) 2985–9614, https://doi.org/10.1002/pola.20789.
[32] N. Hasirci, E.A. Aksoy, Synthesis and modifications of polyurethanes for biomedical purposes, High Perform. Polym. 19 (5–6) (2007), https://doi.org/10.1177/0954008307081203 (621-375-6).
[33] D. Sundaramurthi, U.M. Krishnan, S. Sethuraman, Electrospun nanofibers as scaffolds for skin tissue engineering, Polym. Rev. 54 (2) (2014) 348–762, https://doi.org/10.1080/15583724.2014.881374.
[34] J. Gao, C. Li, J. Zhou, L. Lu, C. Zhao, Y. Zhu, Plasma sprayed alumina–nanosilver antibacterial coatings, RSC Adv. 5 (26) (2015) 20357–26426, https://doi.org/10.1039/C5RA01329A.
[35] M. Liu, A. Guinart, A. Granados, C. Gimbert-Suriñach, E. Fernández, R. Pleixats, et al., Coated cotton fabrics with antibacterial and anti-inflammatory silica nanoparticles for improving wound healing, ACS Appl. Mater. Interfaces 16 (12) (2024) 14595–60412, https://doi.org/10.1021/acsami.4c00383.
[36] F. Zhao, D. Yao, R. Guo, L. Deng, A. Dong, J. Zhang, Composites of polymer hydrogels and nanoparticulate systems for biomedical and pharmaceutical applications, Nanomaterials 5 (4) (2015), https://doi.org/10.3390/nano5042054 (2054-1304).
[37] T.W. Barrowcliffe, Heparin - A Century of Progress 1 ed., XIV, Springer, Berlin, Heidelberg, 2012 (462 p.).
[38] H. Jack, S.A. Sonia, L.H. Jonathan, F. Valentin, Guide to anticoagulant therapy: heparin, Circulation 103 (24) (2001) 2994–301824, https://doi.org/10.1161/01.cir.103.24.2994.

[39] J.K. Shute, E. Puxeddu, L. Calzetta, Therapeutic use of heparin and derivatives beyond anticoagulation in patients with bronchial asthma or COPD, Curr. Opin. Pharmacol. 40 (2018) 39–45, https://doi.org/10.1016/j.coph.2018.01.006.
[40] L. Galvan, Effects of heparin on wound healing, J. Wound Ostomy Continence Nurs. 23 (4) (1996) 224–264, https://doi.org/10.1016/s1071-5754(96)90095-9.
[41] J. Rak, J.I. Weitz, Heparin and angiogenesis: size matters!, Arterioscler. Thromb. Vasc. Biol. 23 (11) (2003), https://doi.org/10.1161/01.ATV.0000100563.16983.19 (1954-511).
[42] P. Wang, L. Chi, Z. Zhang, H. Zhao, F. Zhang, R.J. Linhardt, Heparin: an old drug for new clinical applications, Carbohydr. Polym. 295 (2022) 119818, https://doi.org/10.1016/j.carbpol.2022.119818.
[43] B. Casu, A. Naggi, G. Torri, Re-visiting the structure of heparin, Carbohydr. Res. 403 (2015) 60–68, https://doi.org/10.1016/j.carres.2014.06.023.
[44] D. Cont, S. Harm, C. Schildböck, C. Kolm, A.K.T. Kirschner, A.H. Farnleitner, et al., The neutralizing effect of heparin on blood-derived antimicrobial compounds: impact on antibacterial activity and inflammatory response, Front. Immunol. 15 (2024), https://doi.org/10.3389/fimmu.2024.1373255.
[45] G. Yang, L. Yang, X. Zhou, Inhibition of bacterial swimming by heparin binding of flagellin FliC from Escherichia coli strain Nissle 1917, Arch. Microbiol. 205 (8) (2023) 2868, https://doi.org/10.1007/s00203-023-03622-9.
[46] P. Olczyk, Ł. Mencner, K. Komosinska-Vassev, Diverse roles of heparan sulfate and heparin in wound repair, Biomed. Res. Int. 2015 (2015) 549417, https://doi.org/10.1155/2015/549417.
[47] J. Hogwood, E. Gray, B. Mulloy, Heparin, heparan sulphate and sepsis: potential new options for treatment, Pharmaceuticals (Basel) 16 (2) (2023) 2, https://doi.org/10.3390/ph16020271.
[48] J.M. Oliva, J.M. Ríos de la Rosa, M.J. Sayagués, J.A. Sánchez-Alcázar, P. J. Merkling, A.P. Zaderenko, Solvent-assisted in situ synthesis of cysteamine-capped silver nanoparticles, ANSN 9 (1) (2018) 0150011, https://doi.org/10.1088/2043-6254/aa9de9.
[49] S. Roman, I. Urbánková, G. Callewaert, F. Lesage, C. Hillary, N.I. Osman, et al., Evaluating alternative materials for the treatment of stress urinary incontinence and pelvic organ prolapse: a comparison of the in vivo response to meshes implanted in rabbits, J. Urol. 196 (1) (2016) 261–291, https://doi.org/10.1016/j.juro.2016.02.067.
[50] S. Shafaat, N. Mangir, S.R. Regureos, C.R. Chapple, S. MacNeil, Demonstration of improved tissue integration and angiogenesis with an elastic, estradiol releasing polyurethane material designed for use in pelvic floor repair, Neurourol.Urodyn. 37 (2) (2018), https://doi.org/10.1002/nau.23510 (716-252).
[51] T. Maneerung, S. Tokura, R. Rujiravanit, Impregnation of silver nanoparticles into bacterial cellulose for antimicrobial wound dressing, Carbohydr. Polym. 72 (1) (2008) 43–511, https://doi.org/10.1016/j.carbpol.2007.07.025.
[52] V. Ravichandran, S. Vasanthi, S. Shalini, S.A.A. Shah, M. Tripathy, N. Paliwal, Green synthesis, characterization, antibacterial, antioxidant and photocatalytic activity of Parkia speciosa leaves extract mediated silver nanoparticles, Results Phys. 15 (2019) 102565, https://doi.org/10.1016/j.rinp.2019.102565.
[53] C.S. Miranda, A.F.G. Silva, S.M.M.A. Pereira-Lima, S.P.G. Costa, N.C. Homem, H. P. Felgueiras, Tunable spun fiber constructs in biomedicine: influence of processing parameters in the fibers' architecture, Pharmaceutics 14 (1) (2022) 1641, https://doi.org/10.3390/pharmaceutics14010164.
[54] Z.-M. Huang, Y.Z. Zhang, M. Kotaki, S. Ramakrishna, A review on polymer nanofibers by electrospinning and their applications in nanocomposites, Compos. Sci. Technol. 63 (15) (2003) 2223–5315, https://doi.org/10.1016/S0266-3538(03)00178-7.
[55] H.b. Hashim, N.A.A.b. Emran, T. Isono, S. Katsuhara, H. Ninoyu, T. Matsushima, et al., Improving the mechanical properties of polycaprolactone using functionalized nanofibrillated bacterial cellulose with high dispersibility and long fiber length as a reinforcement material, Compos. Part A Appl. Sci. Manuf. 158 (2022) 106978, https://doi.org/10.1016/j.compositesa.2022.106978.
[56] P. Chen, M. Chai, Z. Mai, M. Liao, X. Xie, Z. Lu, et al., Electrospinning polyacrylonitrile (PAN) based nanofiberous membranes synergic with plant antibacterial agent and silver nanoparticles (AgNPs) for potential wound dressing, Mater. Today Commun. 31 (2022) 103336, https://doi.org/10.1016/j.mtcomm.2022.103336.
[57] H. Lv, S. Cui, Q. Yang, X. Song, D. Wang, J. Hu, et al., AgNPs-incorporated nanofiber mats: relationship between AgNPs size/content, silver release, cytotoxicity, and antibacterial activity, Mater. Sci. Eng. C 118 (2021) 111331, https://doi.org/10.1016/j.msec.2020.111331.
[58] X. Liu, L.H. Nielsen, S.N. Kłodzińska, H.M. Nielsen, H. Qu, L.P. Christensen, et al., Ciprofloxacin-loaded sodium alginate/poly (lactic-co-glycolic acid) electrospun fibrous mats for wound healing, Eur. J. Pharm. Biopharm. 123 (2018) 42–49, https://doi.org/10.1016/j.ejpb.2017.11.004.
[59] S.J. Lee, D.N. Heo, J.-H. Moon, H.N. Park, W.-K. Ko, M.S. Bae, et al., Chitosan/polyurethane blended fiber sheets containing silver sulfadiazine for use as an antimicrobial wound dressing, J. Nanosci. Nanotechnol. 14 (10) (2014) 7488–9410, https://doi.org/10.1166/jnn.2014.9581.
[60] B. Pant, M. Park, G.P. Ojha, D.U. Kim, H.Y. Kim, S.J. Park, Electrospun salicylic acid/polyurethane composite nanofibers for biomedical applications, Int. J. Polym. Mater. 67 (12) (2018) 739–4412, https://doi.org/10.1080/00914037.2017.1376200.
[61] Z. Pedram Rad, J. Mokhtari, M. Abbasi, Preparation and characterization of Calendula officinalis-loaded PCL/gum arabic nanocomposite scaffolds for wound healing applications, Iran. Polym. J. 28 (1) (2019) 51–631, https://doi.org/10.1007/s13726-018-0674-x.
[62] D. Porrelli, M. Gruppuso, F. Vecchies, E. Marsich, G. Turco, Alginate bone scaffolds coated with a bioactive lactose modified chitosan for human dental pulp stem cells proliferation and differentiation, Carbohydr. Polym. 273 (2021) 118610, https://doi.org/10.1016/j.carbpol.2021.118610.
[63] C. Zhang, J.-d. Chen, F.-q. Yang, Konjac glucomannan, a promising polysaccharide for OCDDS, Carbohydr. Polym. 104 (2014) 175–181, https://doi.org/10.1016/j.carbpol.2013.12.081.
[64] F. Abasalizadeh, S. Abasalizadeh, L. Kalafi, Prevalence rate of placenta accreta in women candidates for non-emergency cesarean section with previous cesarean section referred to Tabriz women's hospitals: 2012-2016, Iran. J. Obstet. Gynecol. Infertil. 22 (11) (2020) 1–711, https://doi.org/10.22038/ijogi.2020.14947.
[65] L. Tarusha, S. Paoletti, A. Travan, E. Marsich, Alginate membranes loaded with hyaluronic acid and silver nanoparticles to foster tissue healing and to control bacterial contamination of non-healing wounds, J. Mater. Sci. Mater. Med. 29 (2) (2018) 222, https://doi.org/10.1007/s10856-018-6027-7.
[66] D. Queen, J.D.S. Gaylor, J.H. Evans, J.M. Courtney, W.H. Reid, The preclinical evaluation of the water vapour transmission rate through burn wound dressings, Biomaterials 8 (5) (1987) 367–715, https://doi.org/10.1016/0142-9612(87)90007-x.
[67] J. Drelich, E. Chibowski, Superhydrophilic and superwetting surfaces: definition and mechanisms of control, Langmuir 26 (24) (2010), https://doi.org/10.1021/la1039893 (18621-324).
[68] P. Yu, W. Zhong, Hemostatic materials in wound care, Burns Trauma 9 (2021) 19, https://doi.org/10.1093/burnst/tkab019.
[69] G. Gabbiani, F. Gabbiani, R.L. Heimark, S.M. Schwartz, Organization of actin cytoskeleton during early endothelial regeneration in *vitro*, J. Cell Sci. 66 (1) (1984) 39–501, https://doi.org/10.1242/jcs.66.1.39.
[70] C. Noti, P.H. Seeberger, Chemical approaches to define the structure-activity relationship of heparin-like glycosaminoglycans, Chem. Biol. 12 (7) (2005), https://doi.org/10.1016/j.chembiol.2005.05.013 (731-567).
[71] D.A. Simon Davis, C.R. Parish, Heparan sulfate: a ubiquitous glycosaminoglycan with multiple roles in immunity, Front. Immunol. 4 (2013) 470, https://doi.org/10.3389/fimmu.2013.00470.
[72] M.M. Fuster, L. Wang, Endothelial heparan sulfate in angiogenesis, Prog. Mol. Biol. Transl. Sci. 93 (2010) 179–212, https://doi.org/10.1016/S1877-1173(10)93009-3.
[73] N. Ojeh, K. Hiilesvuo, A. Wärri, M. Salmivirta, T. Henttinen, A. Määttä, Ectopic expression of Syndecan-1 in basal epidermis affects keratinocyte proliferation and wound re-epithelialization, J. Invest. Dermatol. 128 (1) (2008) 26–341, https://doi.org/10.1038/sj.jid.5700967.
[74] A. Asadi, S. Razavi, M. Talebi, M. Gholami, A review on anti-adhesion therapies of bacterial diseases, Infection 47 (1) (2019) 13–231, https://doi.org/10.1007/s15010-018-1222-5.